Preparation of Fluorinated Methacrylate/Clay Nanocomposite via *In-Situ* Polymerization: Characterization, Structure, and Properties

Mohamed Karamane,[1] Mustapha Raihane,[1] Mehmet Atilla Tasdelen,[2] Tamer Uyar,[3] Mohamed Lahcini,[1] Mohamed Ilsouk,[1] Yusuf Yagci[4,5]

[1]Laboratory of Organometallic and Macromolecular Chemistry-Composites Materials Faculty of Sciences and Technologies, Cadi-Ayyad University, Marrakech, 40000, Morocco
[2]Department of Polymer Engineering Faculty of Engineering, Yalova University, Yalova, TR-77100, Turkey
[3]UNAM-Institute of Materials Science and Nanotechnology Bilkent University, Ankara, TR-06800, Turkey
[4]Department of Chemistry Faculty of Science and Letters, Istanbul Technical University, Maslak, Istanbul, TR-34469, Turkey
[5]Center of Excellence for Advanced Materials Research (CEAMR) and Chemistry Department Faculty of Science, King Abdulaziz University, Jeddah, 21589, Saudi Arabia
Correspondence to: M. Raihane (E-mail: m.raihane@uca.ma) or M. A. Tasdelen (E-mail: tasdelen@yalova.edu.tr) or Y. Yagci (E-mail: yusuf@itu.edu.tr)

Received 15 August 2016; accepted 17 October 2016; published online 31 October 2016
DOI: 10.1002/pola.28403

ABSTRACT: Novel fluorinated coating containing well-dispersed silicate nanolayers is successfully produced via *in-situ* free radical polymerization of 2,2,2-trifluoroethyl methacrylate in the presence of vinylbenzyl-functionalized montmorillonite with different loading. The organic modification of sodium montmorillonite is achieved through an ion exchange reaction with triphenylvinylbenzylphosphonium chloride as surfactant prepared before use by reaction with vinylbenyl chloride and phosphine. The following *in-situ* polymerization in the presence of organomodified clay leads to fluorinated nanocomposites with of partially exfoliated and intercalated morphologies, as determined via XRD and TEM analysis. The nanoscale dispersion of clay layers is also evidenced by thermal analysis; a moderate decrease of the glass transition temperature about 2–8 °C compared to their virgin PMATRIF and an improvement of their thermal stability as evidenced by TGA. The wettability of the nanocomposite films is also studied by contact angle measurements with water. The incorporation of organomodified clays not only increases the hydrophobicity of the fluorinated polymers but also improves the surface properties of obtained nanocomposites. Compared the virgin homopolymer, the mechanical properties of the nanocomposites are reduced by addition of organomodifed clay at temperature from 30 to 60 °C, whereas this trend is gradually decreased at higher temperature. © 2016 Wiley Periodicals, Inc. J. Polym. Sci., Part A: Polym. Chem. **2017**, *55*, 411–418

KEYWORDS: nanocomposites; organoclay; radical polymerization

INTRODUCTION Fluoropolymers are a family of high-performance polymers containing fluorine atoms in either main or side chains.[1–3] They exhibit remarkable properties such as high thermal stability and chemical inertness (to solvents, oils, water, acids, and bases), low surface energy (oil and water repellency), dielectric constants, permittivity, water absorptivity and dissipation factor. Furthermore, the presence of the strong C—F bond (mainly linked to the low polarizability and the strong electronegativity of the fluorine atom, to its small van der Waals radius (1.32 Å), and to the strong C—F bond (485 kJ/mol) has a crucial impact on the high resistance to oxidation as well as excellent durability. Because of these outstanding properties, fluoropolymers have found many applications in energy (fuel cell membranes, lithium ion batteries, and photovoltaics), electrical/electronic, construction, aerospace, aeronautics, textile, and automotive industries.[4–6] Fluoropolymers are typically synthesized from homopolymerization of fluorinated monomers or copolymerization of fluorinated monomers with common hydrocarbon monomers via free radical mechanism.[7–11] For fabrication of hydrophobic surfaces, perfluoroalkyl chains have a better potential because the chains are more rigid than *n*-alkyl chains[12], and remain ordered in the bulk and at the surface at higher temperature than *n*-alkyl chains with the same length.[12,13] In particular, comb-shaped polymers with perfluorooctyl (—C_8F_{17}, R_f) side chains[12] show excellent hydrophobicity[14–16] that is related to the ordered arrangement of perfluoroalkyl groups at the

Additional Supporting Information may be found in the online version of this article.

outermost layer. Synthesis of many fluorinated acrylic homopolymers and copolymers were studied for their unique physical properties.[13,17–19]

Recently, a novel strategy has been applied to improve high mechanical, gas barrier, and thermal properties of polymers by addition of a small amount of nanosized inorganic fillers that have one or more dimensions on the nanometer scale (<100 nm). There are three methods to introduce nanofillers into polymer matrix according to the starting materials and processing techniques; solution exfoliation, melt intercalation and *in-situ* intercalative polymerization. Among them, the *in-situ* intercalative polymerization is an effective method to obtain well-dispersed nanofillers in polymer matrix compared with other methods. In this strategy, the nanofiller is swollen with a suitable liquid monomer solution prior to polymerization and then initiated by radiation or heat using a suitable initiator or catalysts.[20–28] The presence of nanofillers during polymerization can increase the interaction between nanofillers and polymers and allow to produce materials with homogeneous dispersion. The layered silicate-based clay minerals are among the most commonly employed inorganic nanofillers because of their abundance, price and well-known intercalation chemistry. Up to date, various combinations of non-fluorinated acrylic matrices [e.g., poly(methyl methacrylate)[27–34], poly(ethyl methacrylate),[35,36] and poly(butyl methacrylate)[37–39]] with different types of organomodified nanoclays via *in-situ* intercalative polymerization have been reported.[40–42]

Here, we report the *in-situ* preparation of fluorinated methacrylate/clay nanocomposites by free radical polymerization. In this method, first, a quaternized ammonium-containing monomer, triphenylvinylbenzyl phosphonium chloride, was first synthesized from triphenylphosphine and vinylbenzyl chloride, then ion-exchanged with sodium montmorillonite (Na-MMT) to obtain organomodified clay (VBz-MMT) containing polymerizable functionality. The *in-situ* polymerization of 2,2,2-trifluoroethyl methacrylate in the presence of VBz-MMT with different loadings by using 2,2′-azobisisobutyronitrile (AIBN) as iniator were initiated by heating the reaction mixture at 70 °C. As a result of the chain growth in between the silicate layers, the ordered silicate layers can be gradually pushed apart one from each other and finally exfoliated in the polymer matrix. By applying this approach, one can easily prepare fluoropolymer/clay nanocomposites with tailor made properties, which expand their usage in material science.

EXPERIMENTAL

Materials

Sodium montmorillonite MMT K10 (Na-MMT, cation exchange capacity = 92 meq/100 g, surface area= 220–270 m^2/g, Alfa Aesar) was purchased and dried for 24 h before use. Triphenylphosphine (99%, Sigma Aldrich) and 4-vinylbenzyl chloride (90%, Sigma Aldrich) were supplied and used as received. The triphenylvinylbenzylphosphonium chloride (VBz-Phos) and organomodified montmorillonite (VBz-MMT) were prepared according to a previously published report.[43] 2,2,2-Trifluoroethyl methacrylate (MATRIF, 99%, Bp, 109 °C/760 mmHg, Sigma Aldrich) and ethyl methacrylate (EMA, Bp, 118–119 °C/760 mmHg, Sigma Aldrich) were distillated at reduced pressure before use. 2,2′-Azobisisobutyronitrile as free radical initiator was purchased from Sigma-Aldrich and purified by recrystallization from methanol. Tetrahydrofuran, methanol and pentane were purchased from Sigma-Aldrich and used as received.

Preparation of PMATRIF/MMT Nanocomposites via *In-Situ* Polymerization

The organophilic clay VBz-MMT (1, 3, and 5% of the monomer by weight) was mixed with monomer (7 g, MATRIF) and dispersed by Ultrason during 45 min. The mixture was then stirred over the night. AIBN (1% wt of the monomer) was added to the mixture and the suspension was degassed with nitrogen prior to polymerization (15 min). The mixture was placed in a thermostated oil bath at 70 °C for 4 h. At the end of the polymerization, the mixture dissolved in THF and precipitated in a large excess of pentane and dried in a vacuum oven at 50 °C for 2 days. Monomer conversions were determined gravimetrically (Yield ~60–80%). For the comparison, the PMATRIF homopolymer and the corresponding non-fluorinated polymer PEMA without clay were prepared by similar procedure.

Characterization

FTIR spectra were recorded from KBr pellets containing 1% by weight of product, using a Perkin–Elmer 1770 instrument with a DTGS detector at a 4 cm^{-1} resolution. X-ray diffraction measurements (CuKa) were made in reflection mode with a Siemens D500 Krystalloflex 810 apparatus, at a scan rate of 1.08°/min. The clay was analyzed as a powder whereas the composites were in the form of disks of 20 mm diameter and 2 mm thickness. The disks were prepared by compression molding of the melt compounded materials. DSC analysis was carried out using Mettler Toledo DSC equipped with a liquid nitrogen cooling system. The sample (8 mg) was heated from −80 to 100 °C at a heating rate of 10 °C/min and followed by a cooling stage from 100 to −80 °C with cooling rate of 10 °C/min. Finally, samples were cooled to room temperature. The data was analyzed to determine the glass transition temperature T_g, melting temperature T_m, and crystallization temperature T_c from two subsequent heating-cooling cycles performed under nitrogen purge flux. TGA was carried out with a Mettler Toledo TGA/SDTA 851 apparatus at a heating rate of 10 °C/min from room temperature up to 700 °C, with nitrogen as the purge gas (60 mL/min). The PMATRIF/clay nanocomposites were sandwiched in two Teflon films which were put between two heated plates of a press at 150 °C under 70 bar for 10 min. The discs of sodium clay (Na^+-MMT) and the corresponding organomodified clay (VBz-MMT) were also performed. The dynamic contact angle measurements were performed with a contact angle goniometer (contact angle system OCA Neurtek Instruments), equipped with a video camera and image

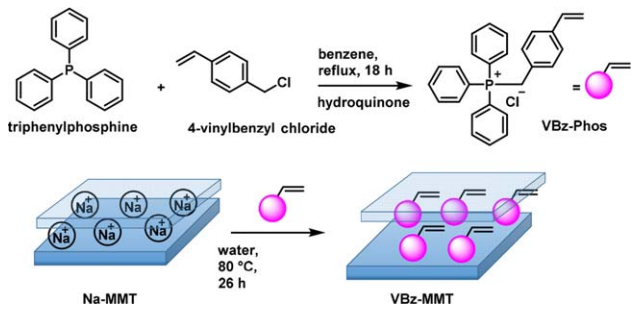

SCHEME 1 Preparation route of organomodified MMT (VBz-MMT). [Color figure can be viewed at wileyonlinelibrary.com]

analyzer, at room temperature with the sessile drop technique. Transmission electron microscopy (TEM) imaging of the samples was carried out on a FEI Tecnai^{TM} G^2 F30 instrument operating at an acceleration voltage of 200kV. Ultrathin TEM specimens (about 100 nm) were prepared by using a cryo-ultramicrotome ($EMUC_6 + EMFC_6$, Leica) equipped with a diamond knife. The ultrathin samples were placed on holey carbon-coated grids for TEM analyses. Dynamic mechanic analysis (DMA) was performed on a ExStar 6100, SII Nanotechnology operating in the tension mode at an oscillation frequency of 1 Hz. Data were collected from room temperature to 300 °C at a scanning rate of 3 °C/min. The sample specimens were cut into rectangular bars, 1 × 20 × 10 mm^3.

RESULTS AND DISCUSSION

Preparation of Vinylbenzyl-Functionalized Montmorillonite (VBz-MMT)

The triphenylvinylbenzylphosphonium chloride salt (VBz-Phos) was prepared according to the synthetic procedure shown in Scheme 1.[43] Its structure was identified by FTIR spectroscopy and differential scanning calorimeter. The characteristic vibration bands at 1436 and 1107 cm^{-1} were assigned to stretching band of $P^+PH_3Cl^-$, whereas the characteristic bands of vinyl and aromatic groups were appeared at 3057, 1587, 1176, and 856 cm^{-1}, respectively. Furthermore, the melting point of VBz-Phos was detected around 142 °C. In the next step, organomodified montmorillonite clay (VBz-MMT) was obtained through an ion exchange reaction between VBz-Phos and Na-MMT. The characteristic absorption bands of both Na-MMT and VBz-Phos were detected in the FTIR spectrum of VBz-MMT (Supporting Information Fig. S1). For example, the bands at 3630 cm^{-1} (valence band of O—H in the species [Al—Al—OH] in octahedral layer of the phyllosilicates), 3414 and 1641 cm^{-1} (stretching and deformation vibrations of hydroxyl group of physisorbed water molecules), 1055 cm^{-1} (large) (elongation vibration of Si—O bond) and 918, 628, 802, and 799.5 cm^{-1} (deformation vibration of (Al, Mg) —OH bond) were corresponded to Na-MMT, whereas the bands at 2931 and 2856 cm^{-1} (symmetric and dissymmetric vibrations of C—H in vinylic band), 1471 and 1116 cm^{-1} (deformation vibrations in the plane and out of plane of $P^+Ph_3Cl^-$), 1600 and 1626 cm^{-1} (stretching bands of C=C in aromatic ring Ar and side vinylic bond —CH=CH_2) and 877 and 844 cm^{-1} (deformation vibrations in the plane and out of plane of C-H band in 1,4-disubtituted aromatic) were assigned to the VBz-Phos. A clear peak shift from 9.0° to 4.2° was detected in the XRD diffractograms of Na-MMT and VBz-MMT. The *d*-spacing of Na-MMT (d_{001}) diffraction peak was 1.0 nm, which was increased to 2.1 nm when modified by VBz-Phos (Supporting Information Fig. S2). Due to the three bulky aromatic rings of VBz-Phos, this increase was higher than aliphatic alkyl ammonium surfactants (i.e., benzyltriethylammonium MMT d_{001}= 1.48 nm).[43]

Thermogravimetric analysis at the temperature range 30–700 °C showed that a mass loss for pure Na-MMT and VBz-MMT of about 11.4% and 30.7%, respectively. For Na-MMT, the 6.5% percentage of mass loss occurred at 30–100 °C, was a result of the release of free water. Whereas, the remaining 4.9% percentage was assigned to the dehydroxylation of structural octahedral hydroxyl groups. For the VBz-MMT, the 1% percentage occurred at 30–100 °C and the remaining 29.7% percentage was assigned to both dehydroxylation of structural octahedral OH and organic VBz-Phos surfactant. Overall, the 24.8% of mass loss corresponds to intercalated monomeric units in the interlayer spaces of MMT. According to equation 1, the loaded amount of the surfactants could be calculated theoretically and was found as 27.6%).[44] The TGA experimental loss was quite consistent with those theoretically predicted value. The FTIR, XRD, and TGA results confirmed that the efficient cation exchange between VBz-Phos and Na+ cations in the galleries of montmorillonite was achieved.

$$Q_{VBz-Phos}(\%) = \frac{(CEC \times M_{VBz-Phos} \times 10^{-3})}{(CEC \times M_{VBz-Phos} \times 10^{-3}) + 100} \times 100 \qquad (1)$$

Preparation of PMATRIF/MMT Nanocomposites via *In-Situ* Polymerization

In-situ polymerization of trifluoroethyl methacrylate (MATRIF) in the presence of different VBz-MMT concentration (1, 3, and 5 wt %) was conducted at 70 °C using AIBN as free radical source. The attachment of monomeric unit enabled to chemical link the growing polymer in the clay platelets through copolymerization. The propagating polymer

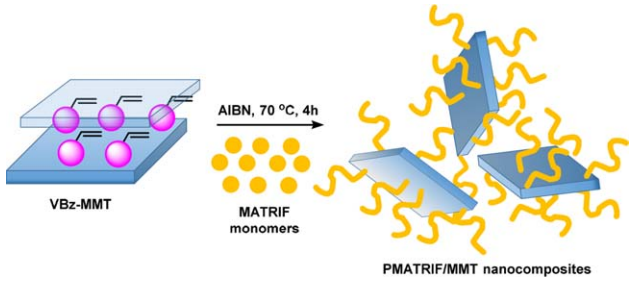

SCHEME 2 *In-situ* preparation of PMATRIF/MMT nanocomposites via thermally initiated free radical polymerization. [Color figure can be viewed at wileyonlinelibrary.com]

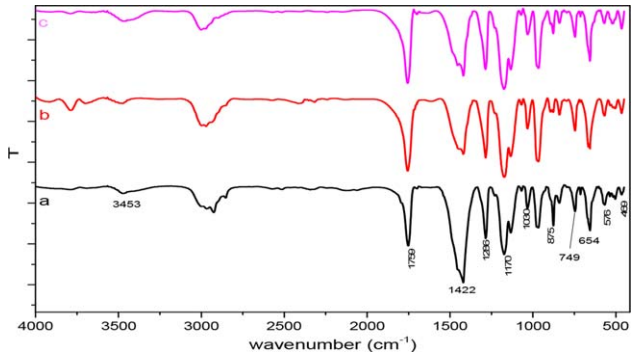

FIGURE 1 FTIR spectra of PMATRIF/MMT nanocomposites: (a) PMATRIF/MMT-1, (b) PMATRIF/MMT-3 and (c) PMATRIF/MMT-5. [Color figure can be viewed at wileyonlinelibrary.com]

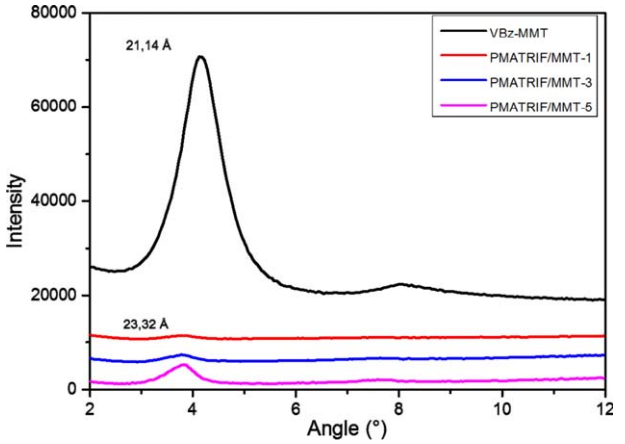

FIGURE 2 XRD diffractograms for VBz-MMT and PMATRIF/MMT nanocomposites. [Color figure can be viewed at wileyonlinelibrary.com]

chains between MMT clay pushed the silicate galleries further apart, which concomitantly resulted in the intercalation as well as exfoliation formations in the nanocomposites. The overall process was depicted in Scheme 2.

The structures of obtained nanocomposites were characterized by FTIR spectroscopy and the frequencies of the vinyl bond (C═C) of VBz-MMT at 1636 cm^{-1} were obviously disappeared indicating the success of the copolymerization of MATRIF and VBz-MMT as well as linking of PMATRIF in the MMT clay galleries. The characteristic absorption bands of PMATRIF were appeared at 3000–2850 cm^{-1} (C—H), 1749 cm^{-1} (C═O), 1459 cm^{-1} (out-of-plane C—H bending) and 1284 and 1183 cm^{-1} (C—O and C—F stretching). All nanocomposite samples (PMATRIF/MMT-1, PMATRIF/MMT-3 and PMATRIF/MMT-5) revealed that both characteristic bands of PMATRIF and VBz-MMT, which were seemed at 1759 cm^{-1} (C═O, strong); 1422 cm^{-1} ($P^{+}Ph_3Cl^{-1}$), and 1030 and 469 cm^{-1} Si—O—Si (Fig. 1). To further confirm the influence of nanoclay on the molecular characteristic of the polymer, a model study in the absence of nanoclay was performed under identical experimental condition. For gel permeation chromatography measurement, the polymer samples from the nanocomposite were obtained after cleaving off from the clay using lithium bromide. By addition of nanoclay, the molecular weights of nanocomposite polymers were significantly decreased compared to the control experiment. In this case, a decreasing order of molecular weights was obtained, showing that the presence of a small concentration of nanoclay acted as chain transfer agent in the polymerization. In addition, the molecular weight distribution of nanocomposite samples was quite similar with the control experiment (Table 1).

Morphological Properties

The XRD diffractograms of VBz-MMT and its nanocomposites loading with 1, 3, and 5% were seen in Figure 2. The *d*-spacing of VBz-MMT (d_{001}) was calculated as 2.10 nm, which was clearly disappeared in the PMATRIF/MMT-1 sample. In the case of PMATRIF/MMT-3 and PMATRIF/MMT-5 samples, broad basal reflections were detected at lower 2-theta angles. The calculated *d*-spacing values were found as 2.33 nm comparatively to 2.10 nm in modified VBz-MMT

TABLE 1 Physical properties of PMATRIF/MMT nanocomposites and their components

Entry	Conversion[a] (%)	d_{001}[b] (nm)	M_n[c] × 10^3 (g/mol)	M_w/M_n[c]	T_g[d] (°C)	Weight loss temperature[e] $T_{d1,10}$ (°C)	$T_{d1,max}$ (°C)	$T_{d2,10}$ (°C)	$T_{d2,max}$ (°C)	Char yield[e] (%)
Na-MMT	–	1.1	–	–	–	–	–	–	–	88.6
VBz-MMT	–	2.1	–	–	–	461.5	483.2	–	–	69.3
PMATRIF	80	n.d.[f]	222	2.3	82.7	250.0	277.9	327.0	358.0	0.7
PMATRIF/MMT-1	66	n.d.[f]	79	1.9	80.1	250.5	275.9	332.8	368.5	1.6
PMATRIF/MMT-3	77	2.3	68	2.3	71.3	251.8	276.5	335.5	375.2	2.5
PMATRIF/MMT-5	61	2.3	42	2.3	70.4	253.3	274.6	339.6	379.8	4.1

[a] Determined by gravimetrically;
[b] Determined by XRD spectroscopy;
[c] Molecular weight and distribution were determined by gel permeation chromatography;
[d] Determined by DSC and analyses under a nitrogen flow at a heating rate of 10 °C/min;
[e] Determined by TGA analysis under a nitrogen flow at a heating rate of 10 °C/min;
[f] Not determined.

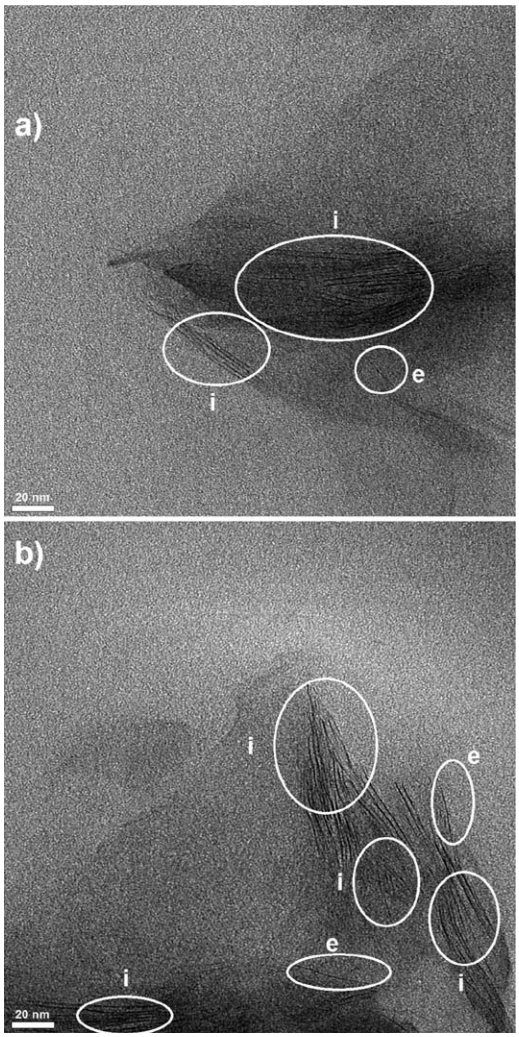

FIGURE 3 TEM micrographs of PMATRIF/MMT-1 and PMATRIF/MMT-3 (scale bar: 20 nm; e: exfoliated and i: intercalated structures).

suggesting intercalated structures in the polymer matrix. In addition, the intensity of the XRD peak was increased with the percentage of VBz-MMT concentration. Due to an increase in clay concentration, the agglomerated clay structures became denser in the polymer matrix and polymer-clay interactions did not overcame the van der Waals forces between silicate interlayers resulting in incomplete delamination of clay layers. Although the intercalated structures were obviously detected with the high clay loadings, the existence of exfoliated structure could not be discounted.

It was previously contended that the sole experimental evidence obtained from XRD was insufficient the complete identification of the nanocomposite structures due to the low volume fraction of nanoclays. It should be supported by transmission electron microscopy (TEM) that was capable of directly identifying the particles that were undetectable using XRD analysis. Thus, supporting TEM analysis was performed for the PMATRIF/MMT-1 and PMATRIF/MMT-3 samples and displayed in Figure 3. In the TEM images, the dark line represented individual silicate layers, whereas the brighter area represents the PMATRIF matrix. The observed individual clay layers (highlighted by black circle and labeled as (**e**) were well dispersed (delaminated), whereas large intercalated tactoids (highlighted by black circle and labeled as (**i**) in the polymer matrix were clearly seen in both samples. Due to the high loading degree or limited mobility of PMATRIF chains within the layers, the small stacks of intercalated MMT layers were occurred.[45–49] Consequently, combined XRD and TEM results confirmed that all nanocomposites had a mixed morphology, in which partially exfoliated/intercalated MMT layers in the PMATRIF matrix.

Thermal Properties

The influence of clay loadings on the glass transition temperatures (T_g) of PMATRIF was investigated by differential scanning calorimetry (Fig. 4). The pure PMATRIF homopolymer and all nanocomposites exhibited a transition from the glassy domain to the viscoelastic one, as evidenced by the presence of only a single T_g, indicating that these materials exhibited amorphous behavior.

All PMATRIF/MMT nanocomposites have lower T_g values (measured at midpoint using DSC) than the pristine polymer PMATRIF ($T_g = 82.7$ °C) prepared under the identical condition. By increasing VBz-MMT loadings, the T_g of PMATRIF/MMT nanocomposites decreased moderately by about 2-12 °C relative to the one of pure PMATRIF and this decrement was less with an increase of clay loading from 3% to 5%. These contradictory results about the clay loading effect on the T_g were also reported in the previously published studies.[50–52] The T_g of PMATRIF ($T_g = 82.7$ °C) was lower than the corresponding non-fluorinated polymer poly(ethyl methacrylate) PEMA ($T_g = 160$ °C)[53] corresponding to plasticizing effect of CF_3 group of MATRIF units comparatively to those of CH_3 alkyl group of PEMA, replacing C—H bond by C—F group reduces the interactions between the main chains and

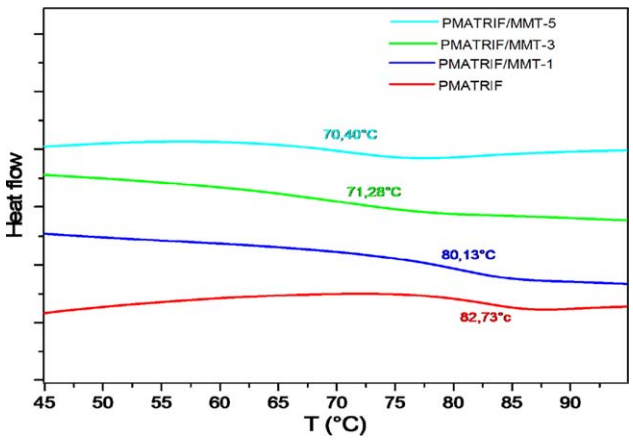

FIGURE 4 PMATRIF/DSC thermograms of pure PMATRIF and MMT nanocomposites with different loadings (heating rate: 10 °C/min under nitrogen atmosphere). [Color figure can be viewed at wileyonlinelibrary.com]

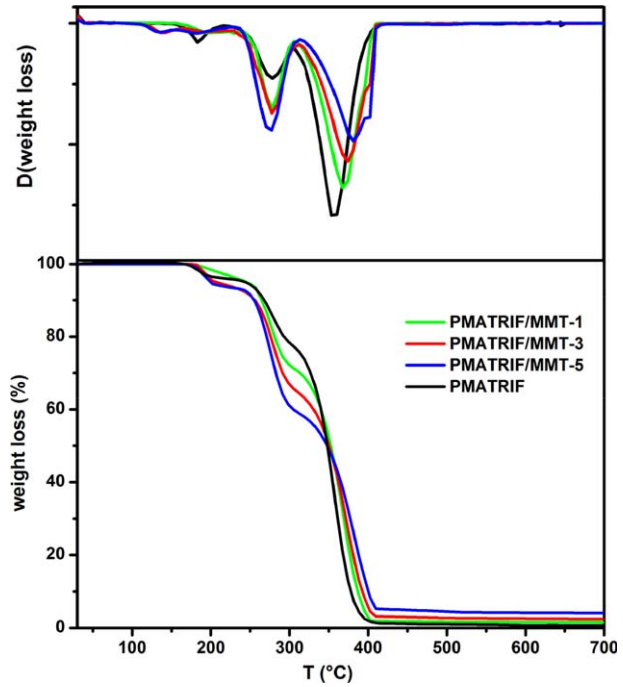

FIGURE 5 TGA (down) and DTG (up) curves of PMATRIF and its different nanocomposites under nitrogen at 10 °C/min. [Color figure can be viewed at wileyonlinelibrary.com]

thus the T_g around 78 °C.[54] The addition of MMT layers reduced the molecular weight of obtained PMATRIF, which could be responsible for the decrease of T_g. The T_g of PMATRIF/MMT nanocomposites ($M_n = 79.000–42.000$ g/mol) were lower than the pure PMATRIF ($M_n = 222.000$ g/mol).

TG analysis of PMATRIF and its corresponding binary nanocomposites was carried out under nitrogen with 10 °C/min heating rate (Fig. 5). The thermal degradation of pure PMATRIF occurred in two main steps (T_{d1} and T_{d2}) in the range of 200–300 °C and 310–500 °C with maximum of thermal decompositions around 277.9 and 358.0 °C. The first decomposition was attributed to the volatilization of side chain fragments including CO_2, vinylidene fluoride, 2,2,2-trifluoroethanol that determined as pyrolytic degradation products.[55,56]

The second degradation corresponded to the depolymerization reaction involving the scission of main chain C—C bonds.[56] The influence of the VBz-MMT nanofiller on the first degradation step was very low as only 3 °C differences between PMATRIF and PMATRIF/MMT-5 in both $T_{d,10}$ (temperature of 10% degradation occurred) and $T_{d,max}$ (temperature of maximum degradation) were observed. In the second step, the thermal stability of the PMATRIF/MMT nanocomposites was improved compared to pure PMATRIF, as was expressed by a shifting of the temperatures degradation to higher temperatures. It was known that the clay layers may act as a heat barrier and consequently contribute to the overall thermal stability of the system.[57] Furthermore, the intercalated or exfoliated nanostructures increase the confinement of polymer chains and inhibited the thermal cracking. The thermogravimetric data of virgin PMATRIF and its corresponding PMATRIF/MMT nanocomposites were summarized in Table 1.

TABLE 2 Measurements of contact angle with water (WCA) of different samples

Entry	WCA (°)
Na^+-MMT	n.d.[a]
VBz-MMT	96.0
PEMA	65.0
PMATRIF	85.5
PEMA/MMT-1	80.0
PMATRIF/MMT-1	90.0
PMATRIF/MMT-3	109.6
PMATRIF/MMT-5	103.0

[a] Not determined.

Surface Properties

In order to investigate the surface properties of obtained nanocomposite, the film samples were prepared by press under 70 bar at 150 °C. The wettability of these films was studied by contact angle measurements with water (WCA) (Fig. 6) and summarized in Table 2.

The WCA of Na-MMT could not be measured because of the high hydrophilic character of the clay that immediately absorbed the water on the surface. The incorporation of three hydrophobic aromatic rings from VBz-Phos into Na-MMT improved the hydrophobicity of the clay surface and the WCA was found as 96°. The contribution of clay on WCA of the nanocomposite surfaces was investigated in two different matrix, either non-fluorinated PEMA or fluorinated PMATRIF. The WCA of pure PEMA was considerably lower than that of PMATRIF through the substitution of C—H bond

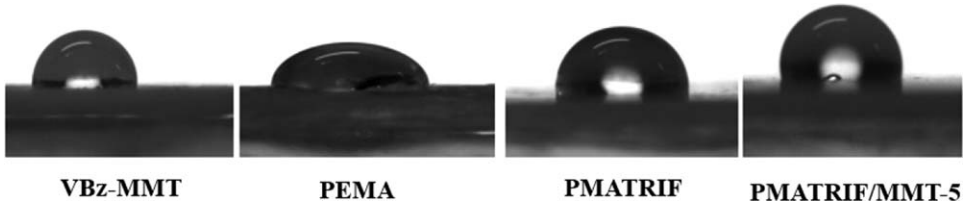

FIGURE 6 Water drop on the surface of the VBz-MMT, PMATRIF (poly(2,2,2-trifluoroethyl methacrylate)), PEMA (poly(ethyl methacrylate)) and its nanocomposites PMATRIF/MMT-5.

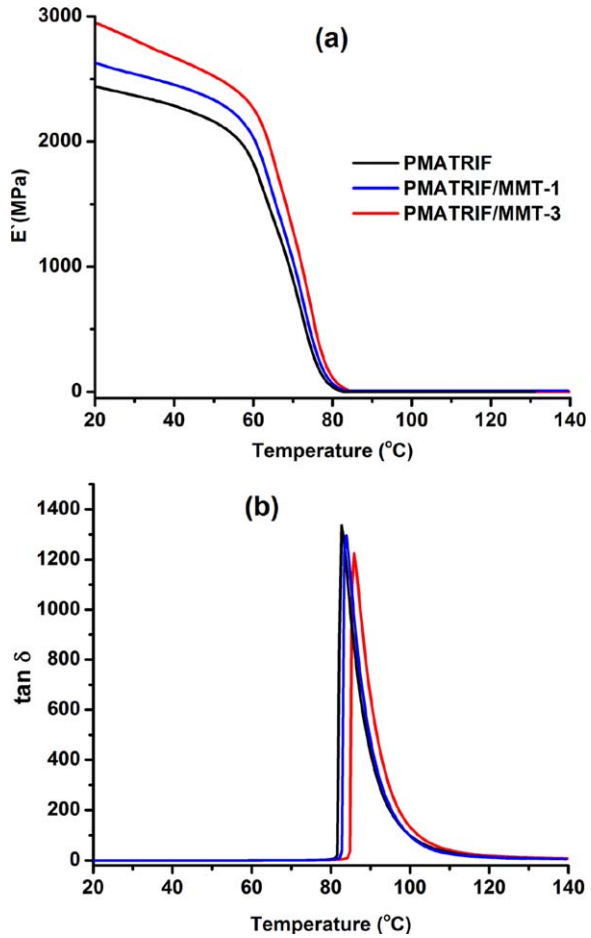

FIGURE 7 Storage modulus versus temperature (a) and loss factor versus temperature (b) curves of PMATRIF and its different nanocomposites. [Color figure can be viewed at wileyonlinelibrary.com]

with C—F bond containing low surface energy of fluorine atoms. In both cases, the addition of MMT clays with 1% ratio into polymer matrix increased the WCA values due to the hydrophobic character of VBz-MMT. This increase is much higher in the non-flourinated PEMA/MMT-1 nanocomposite than in fluorinated PMATRIF/MMT-1 sample. The inclusion of VBz-MMT organomodified clay raises the hydrophobicity of the coatings compared to pure PMATRIF. Similar results were reported by Mokhtar et al.,[58] and Schutzius et al.[59] It is known that WCAs are affected by two factors, that is, surface energy and surface roughness. When the surface is roughened, the change in the liquid surface energy results in two possible contact angles: the Wenzel apparent contact angle,[60] and the Cassie–Baxter apparent contact angle.[61] By changing clay content from 1% to 3, the WCA value was increased with approximately 20°.[62] However, the additional increase of clay loading resulted to a slight decrease with WCA value of PMATRIF/MMT-5. Notably, the higher concentration of the intercalated structures results in agglomeration and also decrease the hydrophobic nature of the film.

Mechanical Properties

The mechanical properties of pure PMATRIF and its nanocomposites were also investigated by dynamic mechanical analysis study and the Young's modulus (E') and tan δ data were presented in Figure 7. The addition of VBz-MMT clay into PMATRIF matrix resulted in a considerable increase of the modulus in both nanocomposite samples compared to pure PMATRIF at temperature from 30 to 60 °C. At higher temperature, this trend between the Young's moduli of the pure PMATRIF and PMATRIF/MMT nanocomposites were gradually decreased. The position of a peak maximum in the tan δ versus temperature was used to determine the T_g of polymers. It was found that the T_g of pure PMATRIF was 81.8 °C, whereas it was slightly shifted to 82.1 and 84.3 °C for PMATRIF/MMT-1 and PMATRIF/MMT-3, respectively. This trend was in contrast with DSC observation that the presence of MMT clays resulted in a decrease of molecular mobility in PMATRIF. In other words, the MMT layers exhibited some physical interactions with the PMATRIF polymer chains to restrict polymer chain motions as well as a decrease in the T_g values.

CONCLUSIONS

In the frame work of developing new fluorinated coating, *in-situ* preparation of PMATRIFTMMT nanocomposites using a MMT modified with VBz-Phos were successfully achieved via thermally initiated free radical polymerization. Depending on the clay concentration, the nanocomposites with mixed morphologies containing partially exfoliated and intercalated structures were obtained as evidenced by XRD and TEM observations. The FTIR analysis also confirmed the presence of MMT layers and PMATRIF homopolymer in all nanocomposites samples. According to DSC and DMA results, the T_g values of nanocomposites slightly reduced about 2–8 °C compared to the virgin PMATRIF, but an improvement of their thermal stabilities was evidenced by TGA. The incorporation of nanoclay with fluorinated polymers improved the hydrophobicity and surface properties of obtained nanocomposites as well. Increase in clay loading leads to a slight decrease in the mechanical properties. These nanocomposites with enhanced physical properties appropriate for many applications such as fuel cell, lithium ion batteries and photovoltaics, electronic, aerospace, textile, and automotive that fluoropolymers are used or likely to be used.

ACKNOWLEDGMENT

The authors would like to thank CNRST (Morocco) - TUBITAK (Turkey) (Project No: 214M013) for financial supports.

REFERENCES AND NOTES

1 L. Du, J. Y. Kelly, G. W. Roberts, J. M. DeSimone, *J. Supercrit. Fluids.* **2009**, *47*, 447–457.

2 B. Améduri, B. Boutevin, Well-architectured fluoropolymers: synthesis, properties and applications; Elsevier: Amsterdam; Boston, **2004**.

3 D. W. Smith, S. T. Iacono, S. S. Iyer, Handbook of fluoropolymer science and technology; Wiley: Hoboken, New Jersey, **2014**.

4 R. Souzy, B. Ameduri, *Prog. Polym. Sci.* **2005**, *30*, 644–687.

5 S. J. Hamrock, M. A. Yandrasits, *Polym. Rev.* **2006**, *46*, 219–244.

6 Z. Cui, E. Drioli, Y. M. Lee, *Prog. Polym. Sci.* **2014**, *39*, 164–198.

7 J. J. Reisinger, M. A. Hillmyer, *Prog. Polym. Sci.* **2002**, *27*, 971–1005.

8 A. Vitale, R. Bongiovanni, B. Ameduri, *Chem. Rev.* **2015**, *115*, 8835–8866.

9 B. Ameduri, R. Bongiovanni, V. Lombardi, A. Pollicino, A. Priola, A. Recca, *J. Polym. Sci. Part A: Polym. Chem.* **2001**, *39*, 4227–4235.

10 B. Ameduri, R. Bongiovanni, G. Malucelli, A. Pollicino, A. Priola, *J. Polym. Sci. Part A: Polym. Chem.* **1999**, *37*, 77–87.

11 A. Priola, R. Bongiovanni, G. Malucelli, A. Pollicino, C. Tonelli, G. Simeone, *Macromol. Chem. Phys.* **1997**, *198*, 1893–1907.

12 T. Doi, Y. Sakurai, A. Tamatani, S. Takenaka, S. Kusabayashi, Y. Nishihata, H. Terauchi, *J. Mater. Chem.* **1991**, *1*, 169–173.

13 E. Martinelli, F. Paoli, B. Gallot, G. Galli, *J. Polym. Sci. Part A: Polym. Chem.* **2010**, *48*, 4128–4139.

14 A. Zaggia, B. Ameduri, *Curr. Opin. Colloid Interface Sci.* **2012**, *17*, 188–195.

15 R. Ishige, T. Shinohara, K. L. White, A. Meskini, M. Raihane, A. Takahara, B. Ameduri, *Macromolecules* **2014**, *47*, 3860–3870.

16 R. Ishige, H. Yamaguchi, T. Shinohara, A. Meskini, M. Raihane, A. Takahara, B. Ameduri, *Polym J.* **2013**, *45*, 1041–1046.

17 E. Martinelli, G. Galli, D. Cwikel, A. Marmur, *Macromol. Chem. Phys.* **2012**, *213*, 1448–1456.

18 E. Martinelli, M. K. Sarvothaman, M. Alderighi, G. Galli, E. Mielczarski, J. A. Mielczarski, *J. Polym. Sci. Part A: Polym. Chem.* **2012**, *50*, 2677–2686.

19 Y. Y. Durmaz, E. L. Sahkulubey, Y. Yagci, E. Martinelli, G. Galli, *J. Polym. Sci. Part a: Polym. Chem.* **2012**, *50*, 4911–4919.

20 C. Dizman, S. Ates, T. Uyar, M. A. Tasdelen, L. Torun, Y. Yagci, *Macromol. Mater. Eng.* **2011**, *296*, 1101–1106.

21 K. D. Demir, M. A. Tasdelen, T. Uyar, A. W. Kawaguchi, A. Sudo, T. Endo, Y. Yagci, *J. Polym. Sci. Part A: Polym. Chem.* **2011**, *49*, 4213–4220.

22 M. A. Tasdelen, *Eur. Polym. J.* **2011**, *47*, 937–941.

23 M. A. Tasdelen, J. Kreutzer, Y. Yagci, *Macromol. Chem. Phys.* **2010**, *211*, 279–285.

24 A. Oral, M. A. Tasdelen, A. L. Demirel, Y. Yagci, *J. Polym. Sci. Part A: Polym. Chem.* **2009**, *47*, 5328–5335.

25 Z. Yenice, M. A. Tasdelen, A. Oral, C. Guler, Y. Yagci, *J. Polym. Sci. Part A: Polym. Chem.* **2009**, *47*, 2190–2197.

26 M. A. Tasdelen, W. Van Camp, E. Goethals, P. Dubois, F. Du Prez, Y. Yagci, *Macromolecules* **2008**, *41*, 6035–6040.

27 H. Akat, M. A. Tasdelen, F. Du Prez, Y. Yagci, *Eur. Polym. J.* **2008**, *44*, 1949–1954.

28 A. Nese, S. Sen, M. A. Tasdelen, N. Nugay, Y. Yagci, *Macromol. Chem. Phys.* **2006**, *207*, 820–826.

29 X. Y. Huang, W. J. Brittain, *Macromolecules* **2001**, *34*, 3255–3260.

30 M. Okamoto, S. Morita, H. Taguchi, Y. H. Kim, T. Kotaka, H. Tateyama, *Polymer* **2000**, *41*, 3887–3890.

31 M. Okamoto, S. Morita, Y. H. Kim, T. Kotaka, H. Tateyama, *Polymer* **2001**, *42*, 1201–1206.

32 P. Meneghetti, S. Qutubuddin, *Langmuir* **2004**, *20*, 3424–3430.

33 A. Oral, M. A. Tasdelen, A. L. Demirel, Y. Yagci, *Polymer* **2009**, *50*, 3905–3910.

34 C. Altinkok, T. Uyar, M. A. Tasdelen, Y. Yagci, *J. Polym. Sci. Part A: Polym. Chem.* **2011**, *49*, 3658–3663.

35 M. N. Siddiqui, H. H. Redhwi, D. Charitopoulou, D. S. Achilias, *Polym. Int.* **2014**, *63*, 766–777.

36 S. Kadi, S. Djadoun, N. Sbirrazzuoli, *Thermochim. Acta.* **2013**, *569*, 127–133.

37 Z. Sedlakova, J. Plestil, J. Baldrian, M. Slouf, P. Holub, *Polym. Bull.* **2009**, *63*, 365–384.

38 M. N. Siddiqui, H. H. Redhwi, K. Gkinis, D. S. Achilias, *Eur. Polym. J.* **2013**, *49*, 353–365.

39 Z. M. O. Rzayev, A. Guner, E. A. Soylemez, S. Kavlak, *J. Appl. Polym. Sci.* **2010**, *118*, 2904–2913.

40 K. Jlassi, M. Benna-Zayani, M. M. Chehimi, Y. Yagci, *J. Polym. Sci. Part A: Polym. Chem.* **2015**, *53*, 800–808.

41 K. Jlassi, S. Chandran, M. Mičušik, M. Benna-Zayani, Y. Yagci, S. Thomas, M. M. Chehimi, *Eur. Polym. J.* **2015**, *72*, 89–101.

42 A. Di Gianni, R. Bongiovanni, L. Conzatti, S. Turri, *J. Colloid Interface Sci.* **2009**, *336*, 455–461.

43 H. El Ghaoui, M. Raihane, B. Rhouta, N. Bitinis, A. Carlmark, M. Arroyo, R. Verdejo, M. A. Lopez-Manchado, M. Lahcini, *Polym. Int.* **2014**, *63*, 709–717.

44 L. Wang, Z. Chen, X. Wang, S. Yan, J. Wang, Y. Fan, *Appl. Clay Sci.* **2011**, *51*, 151–157.

45 M. Arslan, M. A. Tasdelen, T. Uyar, Y. Yagci, *Eur. Polym. J.* **2015**, *71*, 259–267.

46 M. Aydin, T. Uyar, M. A. Tasdelen, Y. Yagci, *J. Polym. Sci. Part A: Polym. Chem.* **2015**, *53*, 650–658.

47 F. B. Barlas, D. A. Seleci, M. Ozkan, B. Demir, M. Seleci, M. Aydin, M. A. Tasdelen, H. M. Zareie, S. Timur, S. Ozcelik, Y. Yagci, *J. Mater. Chem. B.* **2014**, *2*, 6412–6421.

48 M. Aydin, M. A. Tasdelen, T. Uyar, Y. Yagci, *J. Polym. Sci. Part A: Polym. Chem.* **2013**, *51*, 5257–5262.

49 M. Aydin, M. A. Tasdelen, T. Uyar, S. Jockusch, N. J. Turro, Y. Yagci, *J. Polym. Sci. Part a: Polym. Chem.* **2013**, *51*, 1024–1028.

50 J. M. Hwu, G. J. Jiang, Z. M. Gao, W. Xie, W. P. Pan, *J. Appl. Polym. Sci.* **2002**, *83*, 1702–1710.

51 Y. Xu, W. J. Brittain, C. Xue, R. K. Eby, *Polymer* **2004**, *45*, 3735–3746.

52 S. Kumar, J. P. Jog, U. Natarajan, *J. Appl. Polym. Sci.* **2003**, *89*, 1186–1194.

53 S. S. Teixeira, C. J. Dias, M. Dionisio, L. C. Costa, *Polym. Int.* **2013**, *62*, 1744–1749.

54 A. Xu, L. Zhang, J. Ma, Y. Ma, B. Geng, S. Zhang, *J. Coat. Technol. Res.* **2016**, 1–10.

55 P. K. Dhal, G. N. Babu, J. C. W. Chien, *Polym. Degrad. Stab.* **1986**, *16*, 135–145.

56 V. Castelvetro, M. Raihane, S. Bianchi, S. Atlas, I. Bonaduce, *Polym. Degrad. Stab.* **2011**, *96*, 204–211.

57 A. Leszczynska, J. Njuguna, K. Pielichowski, J. R. Banerjee, *Thermochim. Acta.* **2007**, 453–475. *9*, 6.

58 N. M. Mokhtar, W. J. Lau, A. F. Ismail, B. C. Ng, *RSC Adv.* **2014**, *4*, 63367–63379.

59 T. M. Schutzius, I. S. Bayer, M. K. Tiwari, C. M. Megaridis. *Ind. Eng. Chem. Res.* **2011**, *50*, 11117–11123.

60 R. N. Wenzel, *Ind. Eng. Chem.* **1936**, *28*, 988–994.

61 A. B. D. Cassie, S. Baxter, *Trans. Faraday Soc.* **1944**, *40*, 546–551.

62 A. Chakrabarty, S. Ponnupandian, K. Naskar, N. K. Singha, *RSC Adv.* **2016**, *6*, 34987–34995.